Slip-Angle Feedback Control for Autonomous Safety-Critical Maneuvers At-the-Limit of Friction

Victor Fors, Björn Olofsson, & Lars Nielsen
Division of Vehicular Systems, Department of Electrical Engineering
Linköping University, Sweden
E-mail: victor.fors@liu.se

Topics: Vehicle Dynamics and Chassis Control, Advanced Driver Assistant Systems

July 2018

From the basis of optimal control, a closed-loop controller for autonomous vehicle maneuvers at-the-limit of friction is developed. The controller exploits that the optimal solution tends to be close to the friction limit of the tires. This observation allows for simplifications that enable the use of a proportional feedback control in the control loop, which provides a smooth trajectory promising for realization in an actual control system. The controller is in comparison with an open-loop numerical optimal control solution shown to exhibit promising performance at low computational cost in a challenging turn scenario.

1 INTRODUCTION

Active-safety systems have for long been a standard part of road vehicles. Classic examples include the anti-lock braking system (ABS) and the electronic stability control (ESC) system [1]. With the ability for vehicles to detect obstacles ahead, by the use of radar purposed for adaptive cruise control (ACC), collision-avoidance systems are quickly becoming a more common feature. These systems typically work by first issuing a warning to the driver in case of danger, followed by autonomous emergency braking (AEB), if no action is taken by the driver. There is a never-ending increase of autonomy with advanced driver assistance systems (ADAS), which not only control the acceleration and braking, but also control steering to automatically keep the vehicle centered on the road, allowing the driver to temporarily let go of the steering wheel. These functions also call for improvements in collision-avoidance systems and other safety systems that can handle unpredictable safety-critical situations that require combined braking and steering action.

1.1 Background

The problem of collision avoidance by the use of lane-change maneuvers was addressed in [2]. The paper formulated conditions for when it is possible to stop before reaching the obstacle, when it is possible to avoid the obstacle by the use of a lane change, and when a collision is unavoidable. In [3], the strategy obtained by minimum-time optimization of a friction-limited particle model was used in the design of a lane-change control strategy.

To recover from entering a curved road at an excessive velocity, a control law referred to as the parabolic path reference strategy (PPR) was proposed in [4]. The PPR strategy is based on optimal control of a friction-limited particle, where the objective function is to minimize the deviation from the center of the lane. The optimal motion of the particle was shown to be obtained by an acceleration input at-the-limit of friction, in a globally fixed direction. Using the PPR strategy, a complete control concept was developed in [5], where tracking a desired moment is also taken into account. There, a linear combination of the acceleration vector from the PPR strategy and a moment contribution retrieved from an adaptive approach was locally maximized at each individual wheel.

In our previous research [6], which examined optimal braking patterns in safety-critical maneuvers, it was found that optimal solutions for collision avoidance and staying in lane at an excessive velocity share fundamental behavior. It was also noted that for an optimal lane-keeping strategy, the individual tire forces tend to be close to the friction-ellipse limit of the tires, rather than contributing to the turn-in moment of the vehicle by the use of differential braking.

In [7], a low-level steering control for autonomous vehicles was introduced, which tracks the tire-slip angle instead of the more common steering angle. The controller is tested on an autonomous car where improved performance is demonstrated, particularly at the limits of tire friction.

1.2 Contribution

In this paper, a fast to execute closed-loop controller for autonomous maneuvers close to the tire-friction limit is developed. The control is similar in structure to [5], but in comparison to that approach the problem is computationally simplified by exploiting that the solution is close to the friction limit of the tires. This observation results in a control law that enables the use of a low-level feedback control in the control loop with the same structure as introduced in [7]. The closed-loop controller is simulated on a double-track vehicle model that includes roll and pitch dynamics, and the results are compared to those achieved by open-loop numerical optimal control and by an alternate control scheme used in earlier research based on local minimization. The developed controller is shown to provide a smooth trajectory promising for realization in an actual control system, while retaining high performance.

2 CHASSIS CONTROL

The closed-loop control strategy is based on maximizing the acceleration in a globally fixed direction in the spirit of [8, 5]. Different strategies to incorporate yaw-moment control is introduced in [8, 3]. In [9], it was found that close to optimal behavior can be found for some maneuvers by at each time instant momentarily maximizing the force in a globally fixed direction. As a simplification, the closed-loop control strategy does therefore not take yaw-moment control into consideration. With the forces

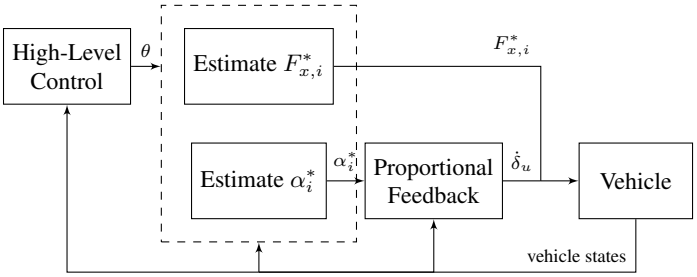

Figure 1: Block diagram of the closed-loop controller.

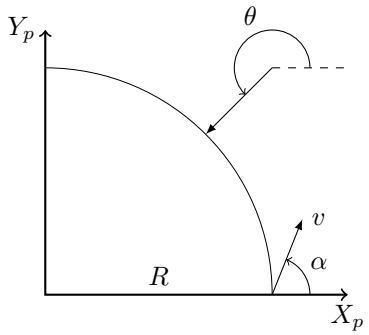

Figure 2: Left-hand turn scenario. θ is the orientation of the globally fixed force vector. α is the orientation of the velocity vector of the vehicle. R is the distance between the vehicle and a globally fixed point marking the center of the turn.

$F_{p,x}$ and $F_{p,y}$ acting on the vehicle in a globally fixed coordinate system, and the fixed orientation $-\pi \leq \theta \leq \pi$ in which the acceleration should be maximized, the problem can mathematically be stated as finding the optimal input u^* in a set of available inputs $u \in U$ as

$$u^* = \arg\max_{u \in U} \underbrace{(F_{x,p}(u)\cos(\theta) + F_{y,p}(u)\sin(\theta))}_{H}. \quad (1)$$

Since (1) is linear in the tire forces, the optimal input can be found individually for each wheel, assuming that the inputs of the wheels are independent from each other. Generating forces from braking is assumed to be faster than the steering response. With that motivation, the problem is split into steering control and braking control parts. A block diagram of the control-system layout is shown in Figure 1.

2.1 High-Level Control

The task of the high-level control is to find in which globally fixed direction to maximize the force according to (1). The left-hand turn scenario illustrated in Figure 2, is used as an example to be solved in the high-level control layer. This is the same scenario as the one examined in [5] and the optimal θ is here estimated using the method presented in that paper. The optimization criterion is to minimize the maximum distance from a globally fixed point that mark the center of the turn, which is equivalent to maximizing the minimum distance from the outer lane border. With the fixed center of the turn defined as the origin, the optimization criterion is

$$\text{minimize}\, X_p^2(t_f) + Y_p^2(t_f), \quad (2)$$

where t_f is the time when maximum distance from the center of the turn is reached, *i.e.*, when the following terminal constraint is fullfilled

$$X_p(t_f)\dot{X}_p(t_f) + Y_p(t_f)\dot{Y}_p(t_f) = 0. \quad (3)$$

The vehicle has the velocity v, where the velocity vector points in an orientation α according to Figure 2. The orientation θ in (1) is estimated by solving the optimization criterion (2) subject to the terminal constraint (3) for a friction-limited particle model

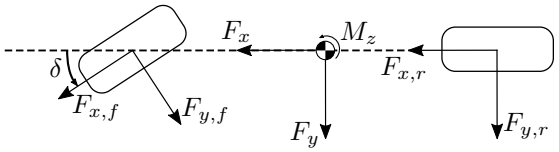

Figure 3: Single-track vehicle model used in the steering control.

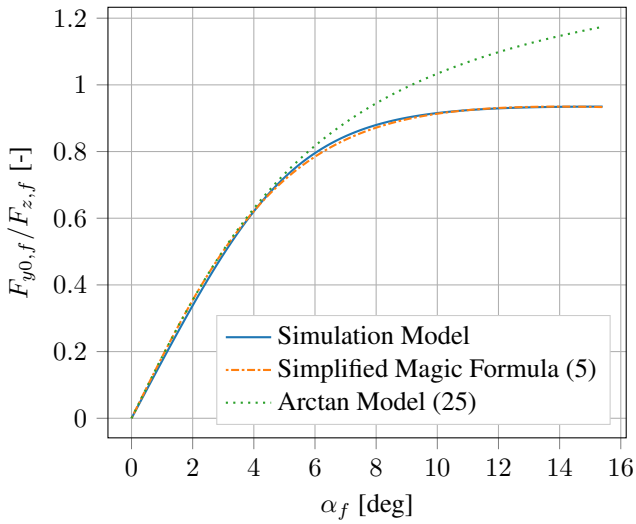

Figure 4: Comparison between different tire models.

with the maximum acceleration μg. Equivalent to the derivation in [5] for the same problem, an algebraic nonlinear equation is obtained, which is solved numerically for θ in the high-level control layer:

$$\frac{2\mu g R}{v^2}\sin(\theta) = \sin(2\theta - 2\alpha). \quad (4)$$

2.2 Steering Control

For the steering control, the vehicle is modeled with the single-track model illustrated in Figure 3. The lateral tire force in the steering control loop is modeled using a simplified version of Pacejka's Magic Formula [10]:

$$F_{y0,i} = \mu_{y,i} F_{z,i} \sin(C_i \arctan(B_i \alpha_i)), \quad (5)$$

where $i \in \{f, r\}$ denotes the front or rear wheel, α_i is the slip angle, and B_i and C_i are tire parameters. Only the range of α_i for which there is a one-to-one correspondence between each α_i and $F_{y0,i}$ is considered. Figure 4 shows a comparison of the simplified Magic Formula used here with the one used in the simulation in Section 4. The slip angles for the front and rear wheel, respectively, are given by [10]

$$\alpha_f = \delta - \arctan\left(\frac{v_y + r l_f}{v_x}\right), \quad (6)$$

$$\alpha_r = -\arctan\left(\frac{v_y - r l_r}{v_x}\right), \quad (7)$$

where v_x is the longitudinal velocity, v_y is the lateral velocity, r is the yaw rate, l_f is the distance from the vehicle center of mass to the front axle, and l_r is the distance from the vehicle center of mass to the rear axle. The longitudinal force $F_{x,i}$ is an input in the model. The effect of combined longitudinal and lateral tire forces is challenging to estimate online. It is thus assumed that the ratio between the lateral force with and without longitudinal slip, $G_{y,i} = F_{y,i}/F_{y0,i}$, is constant between sample instants of the controller. It is assumed that for the single-track model, $F_{y,i}$ can be estimated. Since the ratio $F_{y,i}/F_{y0,i}$ is especially challenging to estimate for small slip angles and small lateral forces, the weight $G_{y,i}$ is saturated in the controller with

$$G_{y,i} = \max\left(\frac{F_{y,i}}{F_{y0,i}}, 0.9\right). \quad (8)$$

2.2.1 *Slip-Angle Reference*

With inspiration from the results in [6], the optimal solution is assumed to be on the friction-ellipse limit. For small changes in α_i, assuming that the friction ellipse is not rotated as a result of changes in the steering angle, the desired lateral tire force $F^*_{y,i}$ is found on the friction-ellipse limit and then (5) is solved backwards to find the desired slip angle α^*_i. The procedure for finding the desired lateral tire force $F^*_{y,i}$ on the friction-ellipse limit is illustrated in Figure 5. The friction-ellipse boundary can mathematically be described by the angle $-\pi \leq \varphi_i \leq \pi$ in the expressions

$$F_{x,i} = \mu_{x,i} F_{z,i} \cos(\varphi_i), \tag{9}$$

$$F_{y,i} = \mu_{y,i} F_{z,i} \sin(\varphi_i). \tag{10}$$

The longitudinal and lateral forces are fully determined by the angle φ_i. The problem (1) can thus be solved by finding the optimal angle

$$\varphi^*_i = \arg\max_{\varphi_i} (\underbrace{\mu_{x,i} \cos(\varphi_i)\cos(\theta_i) + \mu_{y,i} \sin(\varphi_i)\sin(\theta_i)}_{H_{\varphi_i}}), \tag{11}$$

where the angle θ_i is the orientation in which to maximize the tire forces relative to the orientation of each wheel i. This orientation is expressed by the orientation of the vehicle ψ (where $\dot{\psi} = r$) and the steering angle of the wheel δ_i, *i.e.*,

$$\theta_i = \theta - \psi - \delta_i. \tag{12}$$

Differentiating H_{φ_i} from (11) once with respect to φ_i to find extrema gives

$$\frac{\mathrm{d}H_{\varphi_i}}{\mathrm{d}\varphi_i} = -\mu_{x,i} \sin(\varphi_i)\cos(\theta_i) + \mu_{y,i} \cos(\varphi_i)\sin(\theta_i), \tag{13}$$

which is zero when

$$\tan\varphi_i = \frac{\mu_{y,i}}{\mu_{x,i}} \tan(\theta_i). \tag{14}$$

There are clearly two extrema, one on either side of the ellipse. If the extremum is a maximum, the second-order derivate of H_{φ_i} with respect to φ_i should be negative

$$\frac{\mathrm{d}^2 H_{\varphi_i}}{\mathrm{d}\varphi_i^2} = -\mu_{x,i} \cos(\varphi_i)\cos(\theta_i) - \mu_{y,i} \sin(\varphi_i)\sin(\theta_i) < 0. \tag{15}$$

Only braking is allowed, meaning that $|\varphi_i| \geq \pi/2$. Further, the inverse of (5) has to be well defined. To summarize, the following procedure is used to find the desired slip angle α^*_i:

$$\varphi'_i = \arctan\left(\frac{\mu_{y,i}}{\mu_{x,i}} \tan(\theta_i)\right), \tag{16}$$

$$\varphi''_i = \begin{cases} \varphi'_i & \text{if } \frac{\mathrm{d}^2 H_{\varphi_i}(\varphi'_i)}{\mathrm{d}\varphi_i^2} \leq 0, \\ \varphi'_i - \pi \operatorname{sign}(\varphi'_i) & \text{if } \frac{\mathrm{d}^2 H_{\varphi_i}(\varphi'_i)}{\mathrm{d}\varphi_i^2} > 0, \end{cases} \tag{17}$$

$$\varphi^*_i = \begin{cases} \varphi''_i & \text{if } |\varphi''_i| \geq \frac{\pi}{2}, \\ \frac{\pi}{2}\operatorname{sign}(\varphi''_i) & \text{if } |\varphi''_i| < \frac{\pi}{2}, \end{cases} \tag{18}$$

$$\hat{F}^*_{y0,i} = \begin{cases} -1 & \text{if } \frac{\sin(\varphi^*_i)}{G_{y,i}} < -1, \\ \frac{\sin(\varphi^*_i)}{G_{y,i}} & \text{if } -1 \leq \frac{\sin(\varphi^*_i)}{G_{y,i}} \leq 1, \\ 1 & \text{if } \frac{\sin(\varphi^*_i)}{G_{y,i}} > 1, \end{cases} \tag{19}$$

$$\alpha^*_i = \frac{1}{B_i} \tan\left(\frac{1}{C_i} \arcsin(\hat{F}^*_{y0,i})\right). \tag{20}$$

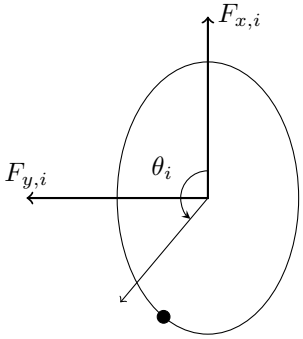

Figure 5: Friction ellipse for a tire. The angle θ_i indicates the direction to maximize the tire forces in. The filled circle indicates the corresponding maximum.

2.2.2 *Slip-Angle Feedback*

A single-track model is used for the steering control; there is thus the front and the rear slip angles to control. Since only the steering angle of the front wheels can be controlled and the optimization criterion (1) is to find the momentarily maximum acceleration, only the front slip angle α_f is controlled. The feedback law for the front slip angle is synthesized as in [7] by the relation

$$\dot{\alpha}_f - \dot{\alpha}^*_f = -K(\alpha_f - \alpha^*_f). \tag{21}$$

The slip angle (6) is simplified by assuming small slip angles for the purpose of being used for feedback. This simplification gives the resulting slip angle and its derivative according to

$$\alpha_f = \delta - \frac{v_y + l_f r}{v_x}, \tag{22}$$

$$\dot{\alpha}_f = \dot{\delta} - \frac{\dot{v}_y + l_f \dot{r}}{v_x} + \frac{\dot{v}_x (v_y + l_f r)}{v_x^2}. \tag{23}$$

From (21) and (23), the desired steering rate $\dot{\delta}_u$ is found as

$$\dot{\delta}_u = -K(\alpha_f - \alpha^*_f) + \dot{\alpha}^*_f + \frac{\dot{v}_y + l_f \dot{r}}{v_x} - \frac{\dot{v}_x (v_y + l_f r)}{v_x^2}. \tag{24}$$

To get an expression to use for the term $\dot{\alpha}^*_f$, a simplified version of the tire model (5) is used in its design:

$$F_{y,f} = \mu_{y,f} F_{z,f} \arctan(B_f C_f \alpha_f). \tag{25}$$

Compared to (5), this tire model does not have zero slope or close to it in the slip range where (5) is valid (see Figure 4). This means that $\dot{\alpha}^*_f$ will be underestimated at larger values of α_f, but should avoid possible undesirable behavior where the estimated value of $\dot{\alpha}^*_f$ gets very large owing to a flat slip–force curve. With the same motivation, effects from combined longitudinal and lateral tire forces are not used either. The derivative of (25) is now calculated to get a linearized tire model of the form

$$F_{y,f} = k_f \alpha_f + \text{constant}, \tag{26}$$

around α^*_f. Assuming that the normal force $F_{z,f}$ changes slowly ($\dot{F}_{z,f} \approx 0$) gives

$$\dot{F}_{y,f} = \mu_{y,f} F_{z,f} \frac{B_f C_f}{(B_f C_f \alpha^*_f)^2 + 1} \dot{\alpha}_f,$$

$$\Rightarrow k_f = \mu_{y,f} F_{z,f} \frac{B_f C_f}{(B_f C_f \alpha^*_f)^2 + 1}. \tag{27}$$

With the simplification $\mu_{x,f} = \mu_{y,f}$ or $\varphi_f = \theta_f$, (10) gives for the linear tire model (26) that

$$\alpha^*_f = \frac{\mu_{y,f} F_{z,f}}{k_f} \sin(\theta_f) + \text{constant}. \tag{28}$$

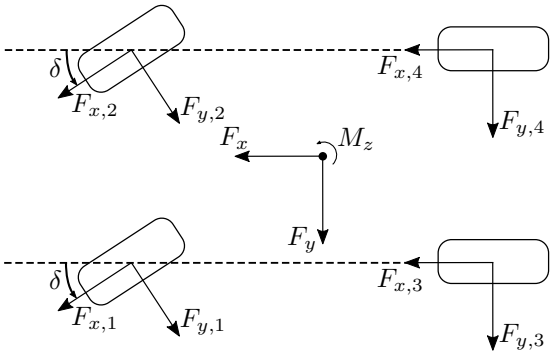

Figure 6: Double-track vehicle model used for the braking control, simulation, and open-loop numerical optimal control.

An approximate expression for the derivative of the desired slip angle can now be found according to

$$\begin{aligned}\dot{\alpha}_f^* &= \frac{\mu_{y,f} F_{z,f}}{k_f} \cos(\theta_f)\dot{\theta}_f \\ &= -\frac{(B_f C_f \alpha_f^*)^2 + 1}{B_f C_f} \cos(\theta_f)(r + \dot{\delta}).\end{aligned} \tag{29}$$

The complete expression for the slip-angle feedback is now found by inserting (29) into (24). Because only braking is considered, $\dot{\alpha}_f^*$ in (24) is set to zero when $|\theta_f| \leq \pi/2$.

2.3 Braking Control

In the braking control, a double-track model (see Figure 6) of the vehicle is considered. The braking control acts individually on each of the four wheels $i \in \{1, 2, 3, 4\}$. The braking torque applied to each wheel is used as the input by approximating that

$$T_{u,i} \approx F_{x,i} R_w, \tag{30}$$

where R_w is the radius of the wheel. To model combined longitudinal and lateral tire forces, the friction-ellipse based relation is used [11]

$$F_{y,i} = F_{y0,i} \sqrt{1 - \left(\frac{F_{x,i}}{\mu_{x,i} F_{z,i}} \right)^2}. \tag{31}$$

This is solved using the same approach as in Section 2.2.1, but where $\mu_{y,i}$ is replaced by $F_{y0,i}/F_{z,i}$. Since braking is the only input, the corresponding φ_i^* is limited to one quarter of the full friction ellipse. For the found φ_i^*, the desired braking force is computed according to (9).

3 SIMULATION & OPTIMIZATION METHOD

A double-track vehicle model with 19 dynamic states, referred to as DT WF in [12], was used for simulation and optimization. To model combined longitudinal and lateral tire forces, weighting functions as suggested in [10] are used. The inputs to the model are the directly applied braking torque $T_{u,i}$ at each wheel $i \in \{1, 2, 3, 4\}$, and the commanded steering rate of the front wheels $\dot{\delta}_u$. The inputs in both simulation and optimization are limited by $|\dot{\delta}_u| \leq \dot{\delta}_{\max} = 1.5$ rad/s and $-\mu_{x,i} R_w F_{z,i} \leq T_{u,i} \leq 0$. The gain K in (24) is set to $K = 19$, which is the same value found to work well in [7] during experiments on a real vehicle.

Enabling a direct comparison, the open-loop numerical optimal control solution of the optimization criterion (2) subject to the terminal constraint (3) is presented alongside the simulation of the closed-loop system using the same vehicle model. To prevent unnecessary actuation in the open-loop numerical optimal control solutions, weights of the form $\eta_i \int_0^{t_f} u_i^2 \, \mathrm{d}t$ for the steering rate and braking torque inputs u_i are added to the optimization criterion (2) when solving the numerical optimal control problem, where η_i for each input is small enough to not influence the maximum deviation as listed in Table 1. The open-loop numerical optimal control problem is solved using the JModelica.org [13] platform.

Table 1: Maximum deviation $e_{\max}$ given the initial velocity v_0 and the initial distance R_0 to the center of the turn.

v_0 [km/h]	R_0 [m]	$e_{\max}$ [m]		
		CL FE	CL LM	OL NOC
70	20	4.49	4.42	4.24
70	30	1.74	1.71	1.62
70	40	0.52	0.52	0.46
70	50	0.21	0.21	0.03
90	40	5.02	4.91	4.70
90	50	2.55	2.49	2.42
90	60	1.07	1.07	1.01
90	70	0.51	0.51	0.41
110	70	4.62	4.51	4.38
110	80	2.68	2.60	2.55
110	90	1.36	1.36	1.31
110	100	0.70	0.71	0.63

Additionally, a comparison of the steering control is made with the control law for the steering angle used in [3]. There, a local maximization of H in (1) (*i.e.*, minimization of $-H$) is performed by using the control law

$$\dot{\delta}_u = \begin{cases} \dot{\delta}_{\max} \operatorname{sign}\left(\frac{\partial H}{\partial \delta}\right) & \text{if } \left|\frac{\partial H}{\partial \delta}\right| > \varepsilon, \\ 0 & \text{otherwise,} \end{cases} \tag{32}$$

where ε is the tolerance. The derivative $\frac{\partial H}{\partial \delta}$ is numerically approximated with the symmetric difference quotient by using small perturbations in the steering angle δ and for the correspondingly perturbed slip angles maximizing H by finding the optimal braking force. The same tire model with weighting functions as used in the simulation is used in this control law. Only the steering control is replaced, the high-level control and the braking control remain the same as described in Section 2. The closed-loop controllers run at 100 Hz in simulation time.

4 RESULTS & DISCUSSION

Three different controllers are compared with each other. They are described in Sections 2–3 and abbreviated as follows:

- CL FE, closed-loop controller using the friction-ellipse based control law in Section 2.2.
- CL LM, closed-loop controller using the local minimization control law (32) from [3].
- OL NOC, open-loop numerical optimal control.

4.1 Performance

In Table 1, results for different initial velocities v_0 and different initial distances R_0 to the center of the turn are listed. The maximum deviation $e_{\max}$ is measured as the maximum distance to the center of the turn subtracted by the initial distance to the center of the turn. It is observed that both closed-loop controllers CL FE and CL LM have almost the same performance, with CL LM performing slightly better. The differences disappear at the respective initial velocity v_0 as the turning radius R_0 gets larger.

The closed-loop controllers take less than one millisecond to execute at each sample on a standard desktop computer, compared to the full numerical optimal control solution that takes up to a minute to solve. Despite this, the closed-loop solutions (CL FE and CL LM) in Table 1 are seen to have comparable performance to the open-loop numerical optimal control solution (OL NOC). Percentagewise, the closed-loop solutions perform

worse at each velocity v_0 as the turning radius R_0 gets larger. The extreme example is for the initial velocity 70 km/h at the initial turning radius 50 m, which is a relatively large turning radius for that initial velocity. In this scenario, the vehicle is, given the available tire–road friction, not traveling at a velocity too excessive to follow a path with curvature according to the initial turning radius R_0. This is thus a scenario more suited for path-tracking controllers, as the desired path can be followed given the available tire–road friction.

4.2 Qualitative Behavior

Figure 7 illustrates the path and the trajectories for the different controllers for the initial velocity $v_0 = 90$ km/h and the initial distance to the center of the turn $R_0 = 40$ m. In the top plot, the paths taken by the controllers are shown and the differences between them are small.

4.2.1 *Steering*

The steering angle δ is in Figure 7 seen to qualitatively share certain behavior between the three controllers. Initially they all increase the steering angle rapidly to a level of approximately 5 degrees and later increase it rapidly again. The developed CL FE controller does not initially increase its steering angle as fast as the other controllers, because of the proportional feedback. While this is detrimental to the performance in this simulated environment, it could potentially be beneficial when implementing it in an actual steering system. The CL LM controller can meanwhile be observed to result in an oscillative steering input, which potentially can be challenging to achieve with the steering actuators when working with an actual steering system.

4.2.2 *Forces and Moment*

Apart from the CL LM controller initially having a larger moment M_z owing to the faster change of steering angle, the closed-loop controllers are observed in Figure 7 to behave very similar in the longitudinal force F_x, the lateral force F_y, and the moment M_z. The oscillations in the steering angle δ in the CL LM controller is seen to largely be averaged out by the dynamics of the vehicle model in the resulting vehicle forces and moment. The OL NOC controller has not only initially larger moment M_z, but also larger F_y in magnitude over the complete maneuver compared to the closed-loop solutions, at the cost of lower F_x in magnitude over the maneuver. This means that the higher initial moment allows the OL NOC controller to use larger lateral tire forces and less braking throughout the rest of the maneuver.

4.2.3 *Braking*

Considering the applied braking torques $T_{u,i}$ in Figure 7, all the controllers behave very similarly, with rear tires being braked almost up until the end of the maneuver where the vehicle reaches its maximum deviation $e_{\max}$. The similarity in the braking torques between the controllers is interesting considering the simple friction-ellipse based model of the combined slip in the closed-loop braking control.

4.2.4 *Slip-Angle Tracking*

In Figure 8, the desired slip angle α_f as computed according to Section 2.2.1 is plotted together with the front slip angle (6). The slip-angle tracking controller is seen to exhibit good performance, though it does not reach zero tracking error during the time that the derivative of the desired slip angle α_f is non-zero. The desired slip angle is seen to change faster and faster before reaching a maximum, corresponding to maximum lateral tire force. Comparing the trajectories for different initial radii R_0, it is seen that a larger R_0 results in the curve being compressed to the left, with a more rapid change in desired slip angle α_f^*.

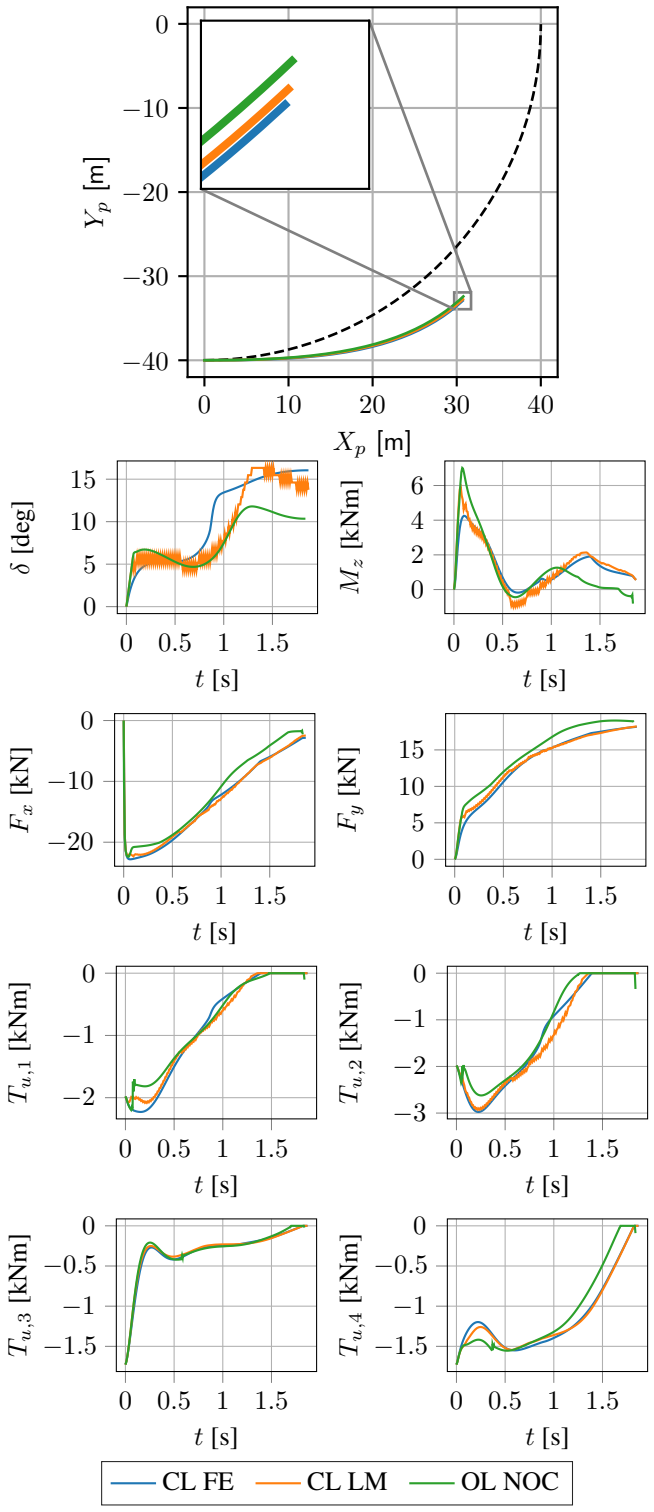

Figure 7: Comparison of open-loop numerical optimal control and the closed-loop controllers for $v_0 = 90$ km/h and $R_0 = 40$ m.

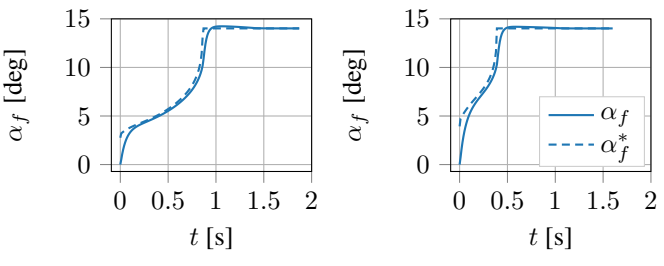

(a) $R_0 = 40$ m (b) $R_0 = 50$ m

Figure 8: Tracking of the desired slip angle α_f^* by the CL FE controller for $v_0 = 90$ km/h at different initial radii R_0.

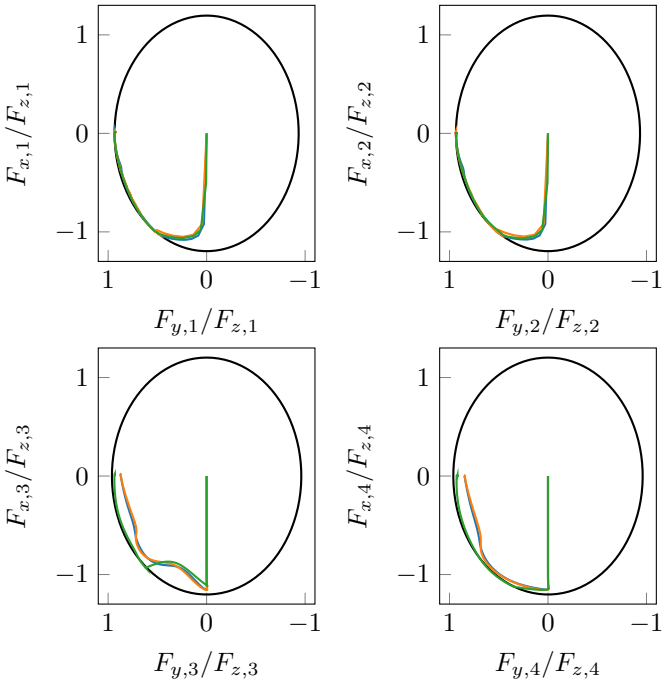

Figure 9: Resulting utilization of the tire forces for each wheel for $v_0 = 90$ km/h and $R_0 = 40$ m. The black line marks the friction-ellipse limits. The colors represent the same controllers as in the legend in Figure 7.

4.2.5 *Tire-Force Utilization*

Figure 9 shows the tire utilization of each tire for the different controllers. The tire utilization of the front tires is very similar, while the utilization of the rear tires differ between the open-loop solution and the closed-loop solutions. The open-loop solution OL NOC is close to the friction-ellipse limit for all four tires, for most of the time. The closed-loop solutions OL FE and OL LM do not travel along the friction limit for the rear tires. The rear slip angles are not controlled in the closed-loop solutions, while they seem to be controlled by the open-loop solution OL NOC to maximum lateral force. This observation explains the higher lateral force of OL NOC observed in Figure 7. Higher lateral force does in this case correspond to higher rear slip angles and thus higher body slip, which may not be desirable.

5 CONCLUSIONS

With the basis in results from optimal control, a fast to execute controller for autonomous maneuvers at the friction limit has been developed, which shows promising performance. Given a globally fixed orientation in which to maximize the force acting on the vehicle (in the spirit of [5, 8, 9]), the steps to calculate the control output are fully explicit, which means that the developed controller can be implemented on very simple hardware.

Closed-loop simulations with the developed controller show how it differs with respect to an open-loop numerical optimal control solution for the same vehicle model and with an alternative control law for the steering proposed and used in earlier research. The performance when comparing the closed-loop controllers is in simulation very similar, but with the developed steering controller offering smoother steering trajectories thanks to the availability of a slip-angle reference signal to track. The smoother steering trajectory could offer benefits in a real-world scenario, where the full steering system has to be considered. When compared with the results from numerical optimal control, the developed closed-loop controller is not far off, but obtained at a significantly lower computational cost.

ACKNOWLEDGMENTS

The authors are members of the ELLIIT Strategic Area for ICT research, supported by the Swedish Government. This work was partially supported by the Wallenberg AI, Autonomous Systems and Software Program (WASP) funded by the Knut and Alice Wallenberg Foundation.

REFERENCES

[1] R. Rajamani. *Vehicle Dynamics and Control*. 2nd edition. New York, United States: Springer, 2012.

[2] Z. Shiller and S. Sundar. “Emergency Lane-Change Maneuvers of Autonomous Vehicles”. In: *ASME Journal of Dynamic Systems, Measurement and Control* 120.1 (1998), pp. 37–44.

[3] Y. Gao, M. Lidberg, and T. J. Gordon. “Modified Hamiltonian algorithm for optimal lane change with application to collision avoidance.” In: *MM Science Journal* MAR 2015 (2015), pp. 576–584.

[4] M. Klomp, M. Lidberg, and T. J. Gordon. “On optimal recovery from terminal understeer”. In: *Proc. Institution of Mechanical Engineers, Part D: J. Automobile Engineering* 228.4 (2014), pp. 412–425.

[5] Y. Gao, T. J. Gordon, M. Lidberg, and M. Klomp. “An autonomous safety system for road departure prevention based on combined path and sideslip control”. In: *Proc. 24th Symp. The Dynamics of Vehicles on Roads and Tracks (IAVSD)*. 2016, pp. 281–286.

[6] V. Fors, B. Olofsson, and L. Nielsen. “A Continuous Family of Optimal Braking Patterns in Autonomous Safety-Critical Maneuvers”. In: *Vehicle System Dynamics* (2018). *Submitted*.

[7] J. K. Subosits and J. C. Gerdes. “A synthetic input approach to slip angle based steering control for autonomous vehicles”. In: *American Control Conference (ACC)*. 2017, pp. 2297–2302.

[8] D. Yang, B. Jacobson, M. Jonasson, and T. J. Gordon. “Closed-loop controller for post-impact vehicle dynamics using individual wheel braking and front axle steering”. In: *International Journal of Vehicle Autonomous Systems* 12.2 (2014), pp. 158–179.

[9] V. Fors. *Optimal Braking Patterns and Forces in Autonomous Safety-Critical Maneuvers*. Linköping Studies in Science and Technology. Licentiate Thesis 1804. Department of Electrical Engineering, Linköping University, Sweden, 2018.

[10] H. B. Pacejka. *Tyre and Vehicle Dynamics*. 2nd edition. Oxford, United Kingdom: Butterworth-Heinemann, 2006.

[11] J. Wong. *Theory of Ground Vehicles*. 4th edition. New York, United States: John Wiley & Sons, 2008.

[12] K. Berntorp, B. Olofsson, K. Lundahl, and L. Nielsen. “Models and methodology for optimal trajectory generation in safety-critical road–vehicle manoeuvres”. In: *Vehicle System Dynamics* 52.10 (2014), pp. 1304–1332.

[13] J. Åkesson, K.-E. Årzén, M. Gäfvert, T. Bergdahl, and H. Tummescheit. “Modeling and Optimization with Optimica and JModelica.org—Languages and Tools for Solving Large-Scale Dynamic Optimization Problems”. In: *Computers and Chemical Engineering* 34.11 (2010), pp. 1737–1749.